Ceramics-Silikáty 66 (3), 296-309 (2022)
www.ceramics-silikaty.cz doi: 10.13168/cs.2022.0026

REPLACEABLE PREFABRICATED CONCRETE-FILLED STEEL TUBULAR NODE

#SHUFENG LI*, GUANGXING LIU**, DI ZHAO*

*School of Civil Engineering, Xuchang University, Xuchang, 461000, China
**Powerchina Eco-Environment Group Co., Ltd, Shenzhen, 518102, China

#E-mail: ll010720@126.com

Submitted April 13, 2022; accepted May 23, 2022

Keywords: Prefabricated concrete filled steel tube, Seismic performance, Oblique bar, Unified theory of concrete-filled steel tube, Shear bearing capacity

A replaceable prefabricated Concrete-filled Steel Tubular (CFST) frame structure is proposed in this paper. The structure has excellent advantages in its construction technology, mechanical behaviour, material application, and post-earthquake recovery and is a green structural system. To explore the seismic performance of the structure, ABAQUS is used to study the influence of different variables on the seismic performance of the node. The hysteretic curve, skeleton curve, stiffness degradation, displacement ductility, and energy dissipation capacity of the node were analysed. The results show that the ductility of this node is basically in a range of 2.02 - 5.75, which is generally higher than 3.0 and has optimal deformation. Furthermore, this node's equivalent viscous damping coefficient is higher than 0.35. In addition, increasing the bolt preload can significantly improve the energy dissipation capacity of the structure in a particular range, and an excessive bolt preload has little effect. Moreover, the high-strength concrete can effectively improve the energy dissipation capacity of the structure. As the axial compression ratio increases, the equivalent viscous damping coefficient has an obvious upward trend. Finally, the stress mechanism of this node was comprehensively analysed according to the theory of oblique bars, the unified theory of concrete-filled steel tubes, and the Kupfer-Gerstle yield criterion, considering the influence of steel tubes on the core concrete.

INTRODUCTION

Concrete-filled steel tubular (CFST) structures are widely used for their high bearing capacity, good plasticity, good fire resistance and optimal seismic performance. With the reform and upgrade of construction in China, prefabricated buildings have become the development trend. In order to give full place to the advantages of CFST, it is of great practical significance to develop prefabricated CFST structures. Ajith et al. [1] conducted an experiment on the hysteretic behaviour of the nodes between CFST columns and steel beams connected by extended end plates with bolts. The test results were analysed in terms of the strength, stiffness, ductility, failure mode and energy dissipation. The results showed that the seismic performance of the structure complied with the seismic recommendations of the American Institute of Steel Construction (AISC), where the combination of tension bolts significantly improved the seismic performance of the structure. Kukla and Kozlowski [2] conducted experiments on six extended and flush end plate joints to understand the actual behaviour of the joints under loads based on bending moments and tensions generated by catenary action. Finite element software was used for the variable-parameter analysis to study the effects of the end plate arrangement and thickness, and the number, location and grade of the bolts. The results showed that the bearing capacity and rotational capacity of the nodes can be improved and the stability of the structure can be enhanced by a symmetrical extended end plate structure. The application of thin end plates reduced the resistance and deformation capacity of the nodes, so as to reduce the rotation ability. A larger bolt diameter can significantly increase the ultimate bearing capacity and avoid brittle failure modes of the node. Additionally, the highest bolt grade (i.e., 12.9) has a positive effect on final joint performance. Extensive studies have also been carried out on traditional bolted end plate joints [3-6] and design methods in different codes, to provide practical design procedures that guarantee resistances and ductility [7-8]. Wang et al. conducted a pseudo-static test on three CFST linking column high-strength bolted end plate joint specimens. The effects of the axial compression ratio, concrete strength, high-strength bolt pretension, end plate thickness and end plate stiffeners on the hysteretic performance of the nodes were studied. The test results showed that the high-strength bolted end plate node had good strength, stiffness, ductility and energy dissipation capacity. In order to study the

seismic performance of the CFST frame under this node, ABAQUS was used for the non-linear numerical analysis of the test specimens. The results showed that the frame hysteresis curve was plump and had good ductility and energy dissipation capacity. When the axial compression of the frame column was relatively small, an ideal beam hinge failure mechanism can be formed. Increasing the thickness of the end plate can improve the stiffness and bearing capacity of the structure, where high-strength bolt pretension had no significant effect on the frame [9-10]. Li et al. conducted an experimental study on a new lightweight steel-concrete composite node. The seismic performance of 4 groups of 8 honeycomb beam-welded ring stirrup-column composite nodes with different connection forms of 1/2 ratio was carried out. Comparing the test, the energy consumption of the bolt connected specimen with the overhanging end plate increased the fastest, and the stirrups, longitudinal reinforcement and concrete in the core area can fully play their roles. Therefore, the bolt connected joint with the overhanging end-plate is a more reasonable node mode [11]. Ding et al. proposed a new type of connection system with a steel beam and concrete-filled steel tube column. This type of connection system uses internal stiffeners and high-strength threaded steel rods to connect the steel beams in two directions with the assistance of side plates pre-welded on the column. The results of experimental and numerical investigations indicate the proposed connection system offers satisfactory stiffness and load-carrying capacities [12].

It can be seen from research that the high-strength bolted connections have good mechanical properties. Based on this information, this paper applies this connection method to the prefabricated CFST structure,

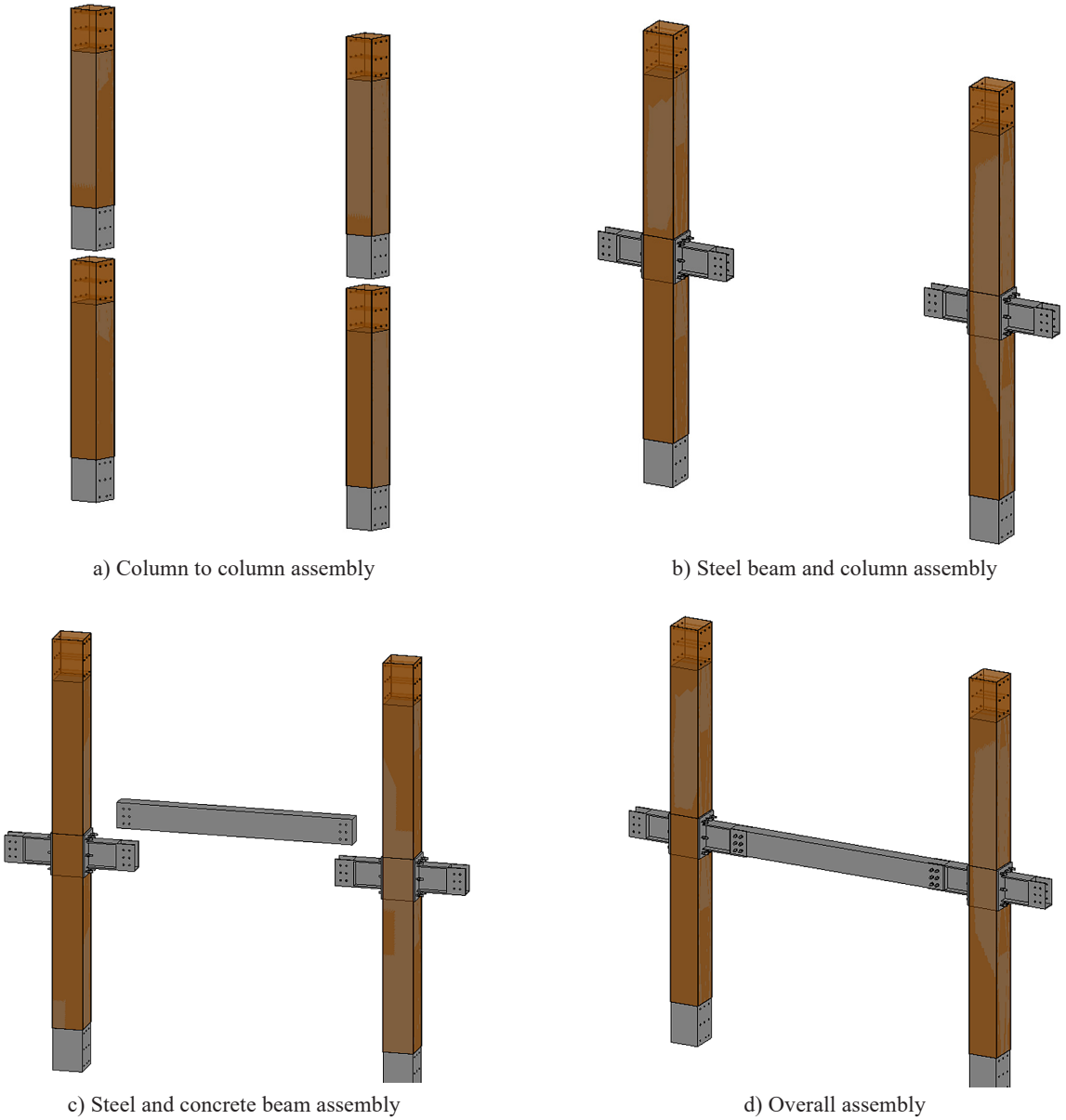

a) Column to column assembly

b) Steel beam and column assembly

c) Steel and concrete beam assembly

d) Overall assembly

Figure 1. Assembly process diagram of the replaceable prefabricated CFST frame structure

and proposes a replaceable prefabricated CFST frame structure. In this structure, the column-to-column connection and the beam-to-column connection are concentrated at the beam-to-column node. In this way, the connection type and number of the structure is reduced and the force transmission path is clear. The construction process of the structure is shown in Figure 1. First, the CFST column is assembled. In the core area of the node, the lower CFST column is poured with concrete, and the upper column extends part of the concrete, so that the concrete protruding from the upper column is placed into the steel pipe reserved for the lower column to complete the column-to-column assembled connection. Then, the end plate-steel beam and column are assembled together by high-strength bolts. Finally, the concrete beam is lapped on the reserved support part of the steel beam, and the concrete beam and the steel beam are connected by high-strength bolts. The structure does not require the on-site pouring of concrete or welding. It is mainly connected by high-strength bolts for the easy positioning of the components. Since the CFST columns, concrete beams, and steel beams are all connected by high-strength bolts, after an earthquake, the corresponding components can be quickly replaced and immediately put into use according to the actual situation of structural damage and for low economic losses.

EXPERIMENTAL

Specimen design and model establishment

A total of 7 specimens were designed in this study, and the specimens are numbered #PAN-01 to #PAN-07. The parameters are mainly the axial compression ratio, concrete strength grade and bolt preload. The cross-sectional dimension of the column is 500 mm (length) × 500 mm (width) × 2800 mm (height); the beam section size is 200 mm (width) × 436 mm (height) × 1800 mm (length); the length of the steel beam is 500 mm; the diameters of the bolt, steel bar and stirrup are 30 mm, 20 mm and 5 mm, respectively. The material properties of the nodes are Q345 grade steel, M20 high-strength bolts and HRB400 steel bars. The basic parameters of the specimens are shown in Table 1.

Table 1. Specimen parameters.

Number	Concrete strength grade	Bolt preload (kN)	Axial pressure ratio
#PAN-01	C30	200	0.3
#PAN-02	C30	300	0.3
#PAN-03	C30	400	0.3
#PAN-04	C40	200	0.3
#PAN-05	C50	200	0.3
#PAN-06	C30	200	0.5
#PAN-07	C30	200	0.7

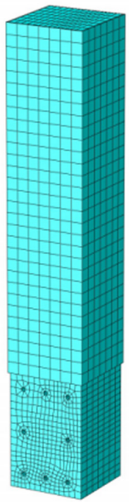

a) Upper half of the concrete column with clad steel

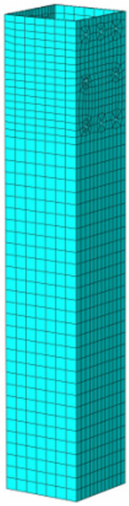

b) Lower half of the concrete column with clad steel

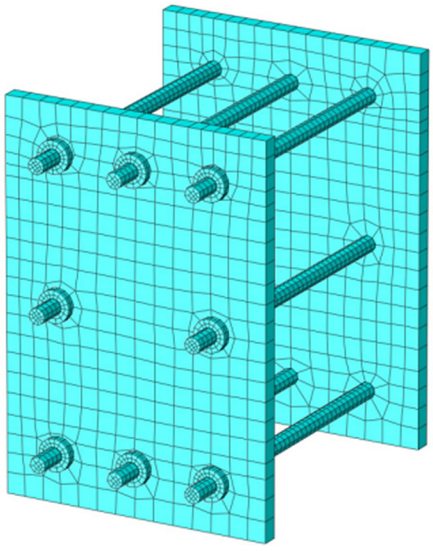

c) Column bolts and end plates

Figure 2. Grids of each part. *(Continue on next page)*

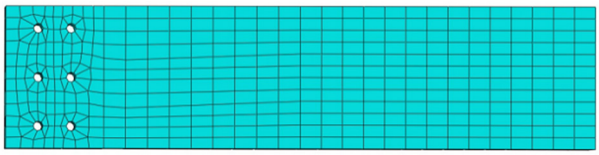

d) Concrete beam

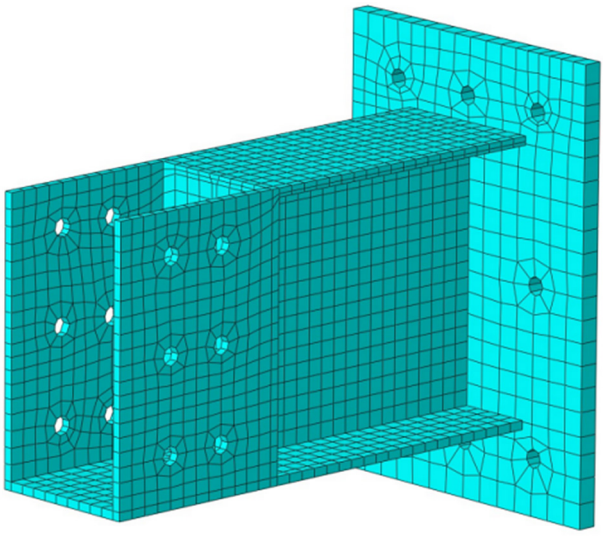

e) Beam end support

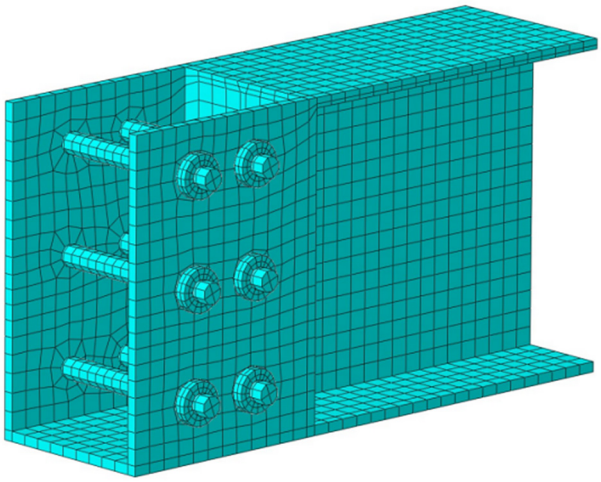

f) Beam bolts

Figure 2. Grids of each part.

When determining the boundary conditions, the lower end of the concrete column will adopt a fixed hinge, that is, the lower end will limit the translation in three directions. The ends of the concrete beams are connected by tie rods, that is, to limit the translation in the vertical direction. Meanwhile, the top and bottom of the column and both ends of the beam are constrained by a coupling to facilitate the application of loads. The displacement control loading method is adopted, and each stage is cycled once. The concrete, end plates, steel pipes and bolts use C3D8R solid elements, and the reinforcement and stirrups use T3D2 truss elements. The interaction between the reinforcement and concrete is defined as "embedded". The tangential directions between the end plate and steel pipe, the steel hoop and column are defined as frictional contact. The penalty function is adopted, and the normal direction is hard contact without penetration. The tangential directions between the bolt and column, the steel plate hoop and end plate are defined as frictional contact. The friction coefficient of the penalty function is 0.6 [13-14]. The reinforcement uses the bi-broken line model and the concrete uses the plastic damage model [15]. The selection of the grid size is mainly based on the stress characteristics of the structure, and the grids are divided more densely in the key parts of the structure under stress [16-17]. The grids of the bolt, end plate, steel bar, beam and column are 8 mm, 35 mm, 50 mm, 70 mm and 70 mm, respectively. The grid division diagram is shown in Figure 2.

RESULTS

Test results and analysis

Hysteresis curve

The hysteresis curves of the seven high-strength bolted end plate connected concrete beam-column assemblies constructed in this paper are shown in Figure 3.

Generally, the hysteretic curve of each specimen has similar characteristics, which basically belong to a shuttle shape. The hysteretic loop is relatively full and has a good energy dissipation capacity. The main reason is that the steel beam is used near the column end. In the initial stage of loading, all the parts of the specimen are in an elastic stage. The load displacement changes linearly and there is basically no residual deformation. With a continuous increase in the load, the damage continues to appear and develop. The stiffness obviously degrades, and the residual deformation becomes large. In the later

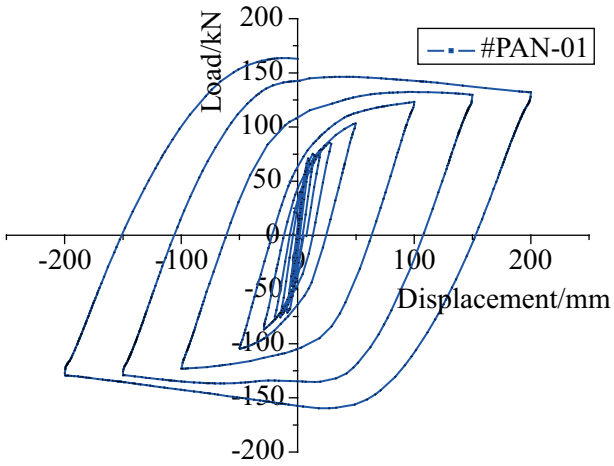

a) Load-displacement curve of #PAN-01

Figure 3. Hysteretic curves of each specimen. *(Continue on next page)*

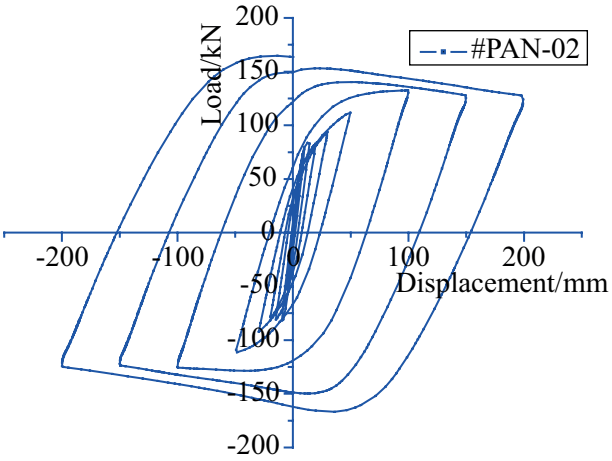

b) Load-displacement curve of #PAN-02

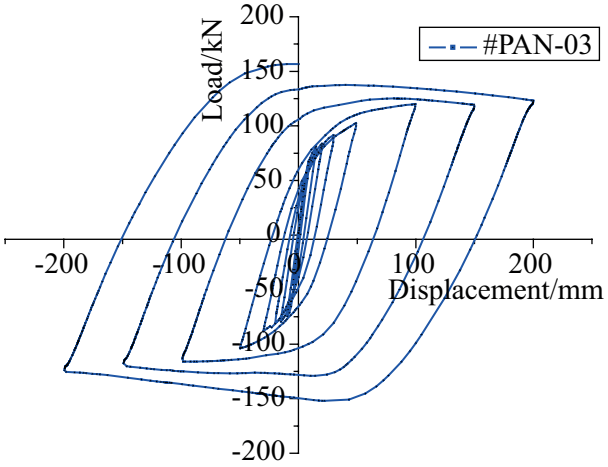

c) Load-displacement curve of #PAN-03

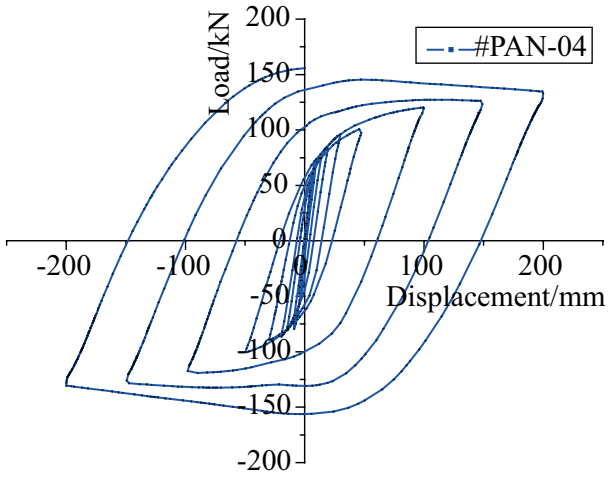

d) Load-displacement curve of #PAN-04

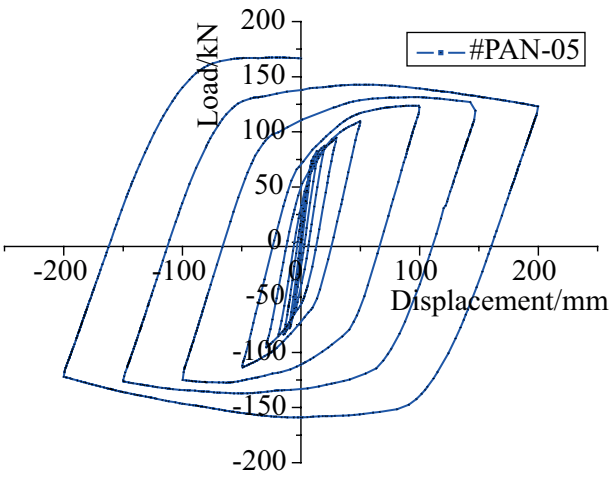

e) Load-displacement curve of #PAN-05

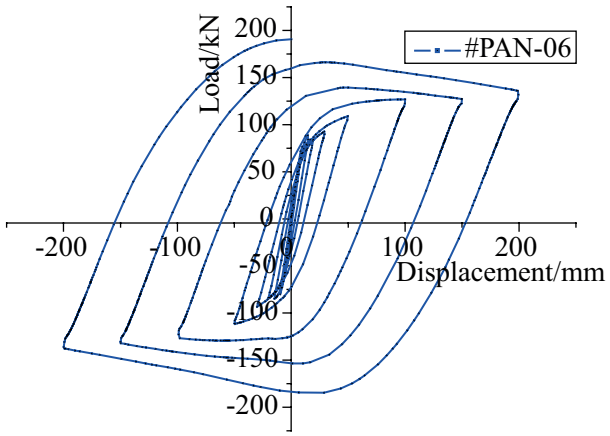

f) Load-displacement curve of #PAN-06

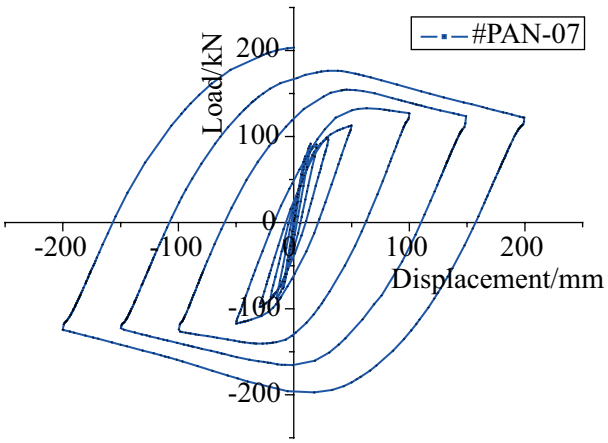

g) Load-displacement curve of #PAN-07

Figure 3. Hysteretic curves of each specimen.

stage of loading, the specimen also has a certain "pinch" phenomenon, and it is not obvious compared with the general cast-in-place nodes. The structure shows good hysteresis characteristics.

Comparing the hysteresis curves of different groups, it can be found that:

- From the hysteresis curves of #PAN-01, #PAN-02 and #PAN-03, it can be seen that with a continuous increase in the bolt preload, the hysteresis loop of the node has a certain increase, but it is not an obvious one. The value of the failure displacement changes slightly and there is no significant decrease after the

peak load. It has good ductility, but the ultimate load decreases to a certain extent.

- From the hysteresis curves of #PAN-01, #PAN-04, #PAN-05, it can be seen that with an increase in the concrete strength, the bearing capacity also increases. #PAN-05 has a fuller hysteresis loop and better seismic performance.
- From the hysteresis curves of #PAN-01, #PAN-06 and #PAN-07, when the axial pressure ratio is relatively high, with a gradual increase in the axial pressure ratio, the hysteresis curve of the node becomes more and more full. This shows that with an increase in the axial compression ratio, the bearing capacity and ductility of the nodes are improved, and the energy dissipation capacity of the structure gradually increases.

Skeleton curve

The skeleton curve of each specimen is shown in Figure 4.

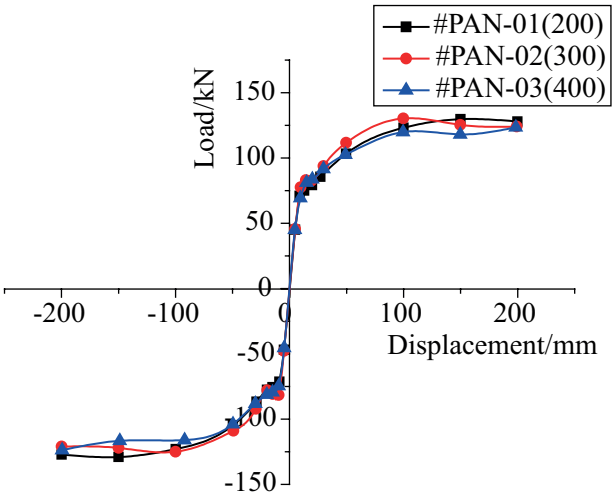

a) Different pre-tightening forces

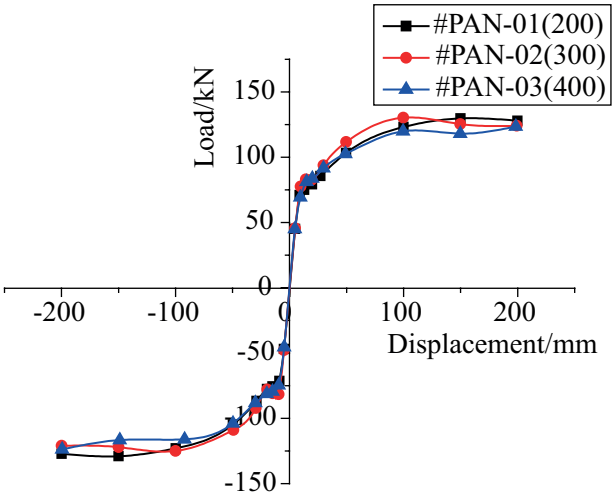

b) Different concrete strengths

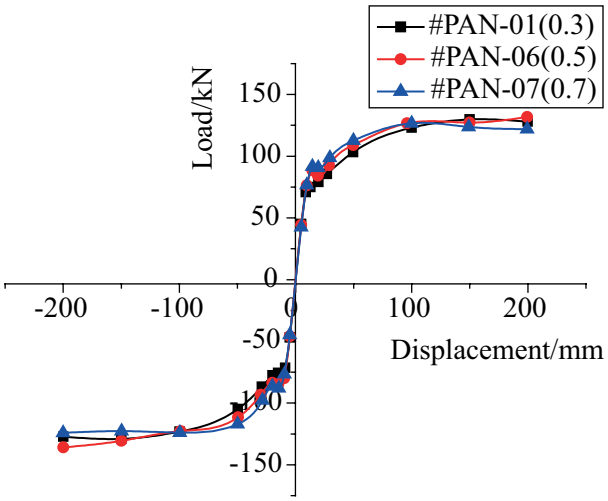

c) Different axial compression ratios

It can be seen from Figure 4 that the skeleton curve of the prefabricated node under the horizontal and low cycle reciprocating load is roughly the same, and it has four stages of elasticity, yielding, strengthening and descending. In the initial stage of loading, the skeleton curve is close to a straight line, and the deformation of the structure is in the elastic range. After the structure is deformed, the slope of the skeleton curve gradually decreases, and the load increases slowly as the displacement increases.

- Comparing the load-displacement skeleton curves of the different bolt preloads, it can be found that the skeleton curves of the nodes are basically the same when the different bolt preloads are applied. When the bolt preload is 300 kN, the ultimate bearing capacity slightly increases. This indicates that increasing the bolt preload to a certain range can improve the bearing capacity of the structure, but not obviously.
- Comparing the load-displacement skeleton curves of the different concrete grades, it can be seen that when the concrete strength grade is C50 and the displacement is about 100 mm, the structure reaches the ultimate bearing capacity. The ultimate bearing capacity of the other two specimens appears later, indicating that the high-strength concrete can weaken the ability of the structure to resist deformation.
- Comparing the load-displacement skeleton curves with the different axial compression ratios, it can be seen that under the action of a high axial compression ratio of 0.7, the skeleton curve is basically above the other two skeleton curves at the early stage of loading. However, in the later stage of loading, its skeleton curve is below the other two skeleton curves. It indicates that a high axial compression can improve the stiffness of the structure in the early stage, but it has an adverse effect on the structure in the later stage.

Figure 4. Comparison of the skeleton curves under different acting parameters.

Ductility

The ductility coefficient of each specimen is shown in Table 2.

It can be seen from Table 2 that the ductility coefficient of this node is basically between 2.02 and 5.75, which is generally higher than 3.0. The assembly has good ductility and deformation ability, and meets the ductility design requirements of the structure. In addition, the yield load, yield displacement, ultimate load and failure displacement of #PAN-06 are higher than the other specimens, and the ductility shows a downward trend with an increase in the bolt preload.

Energy consumption

The existing literature showed that the equivalent viscous damping coefficient of the reinforced concrete nodes was about 0.1, and that of a pure steel frame structure was about 0.2. From Figure 5, the equivalent viscous damping coefficient of the specimen is generally higher than 0.35 when the node fails, and it has a good energy dissipation capacity. From the comparison chart of the equivalent viscous damping coefficient of the different bolt preloads, it can be seen that when the bolt preload is 300 kN, the equivalent viscous coefficient is the largest. This shows that, in a certain range, increasing the bolt preload can greatly improve the energy dissipation capacity of the structure, and an excessive bolt preload has little effect. From the comparison chart of the equivalent viscous damping coefficient under the different concrete strength grades, it can be seen that when the concrete strength grade changes from C30 to C40, the equivalent viscous damping coefficient does not change significantly. However, it increases greatly when the concrete grade is C50. Thereby, the high-strength

Table 2. Ductility coefficient of each specimen.

Number		Yield load P_y (kN)	Yield displacement Δ_y (mm)	Ultimate load P_u (kN)	Failure displacement Δ_u (mm)	Ductility coefficient μ
#PAN-01	Positive	107.48	59.24	129.78	149.85	2.53
	Negative	-129.38	-52.60	-128.95	-149.99	2.85
#PAN-02	Positive	106.27	44.00	130.29	99.74	2.27
	Negative	-104.97	-44.15	-125.02	-99.95	2.26
#PAN-03	Positive	99.47	43.15	123.506	92.63	2.15
	Negative	-101.15	-45.86	-123.79	-92.84	2.02
#PAN-04	Positive	104.45	53.18	132.822	199.76	3.76
	Negative	-106.41	-60.91	-130.58	-199.85	3.28
#PAN-05	Positive	100.14	36.46	123.727	93.72	2.57
	Negative	-103.17	-37.71	-125.02	-99.77	2.65
#PAN-06	Positive	108.38	49.21	131.82	199.35	4.05
	Negative	-112.90	-52.34	-135.98	-199.78	3.82
#PAN-07	Positive	101.99	34.16	126.66	99.92	2.93
	Negative	-103.51	-34.79	-124.16	-199.96	5.75

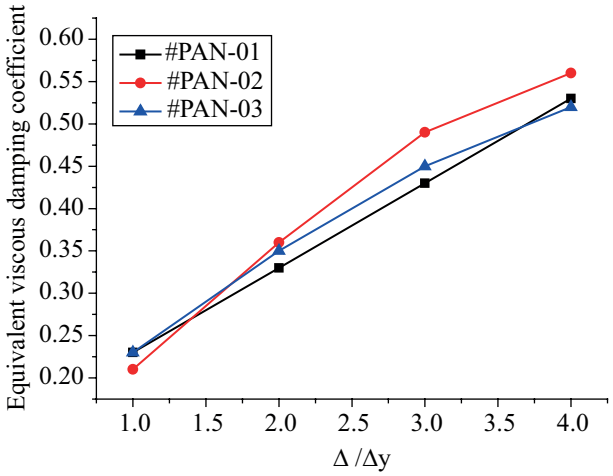

a) Comparison of the equivalent viscous damping coefficients of the different bolt preloads

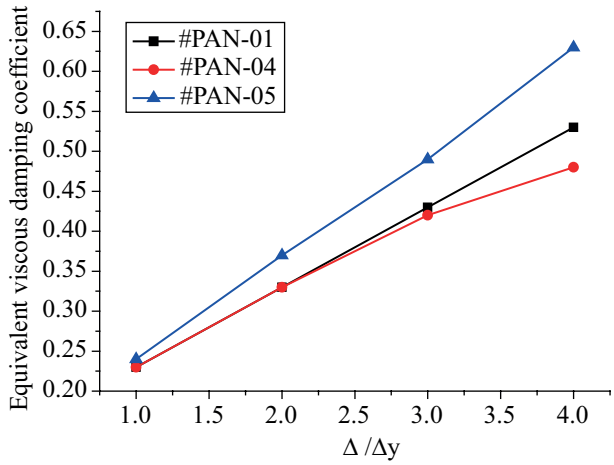

b) Comparison of the equivalent viscous damping coefficients of the different concrete strengths

Figure 5. Comparison of the equivalent viscous damping coefficients. *(Continue on next page)*

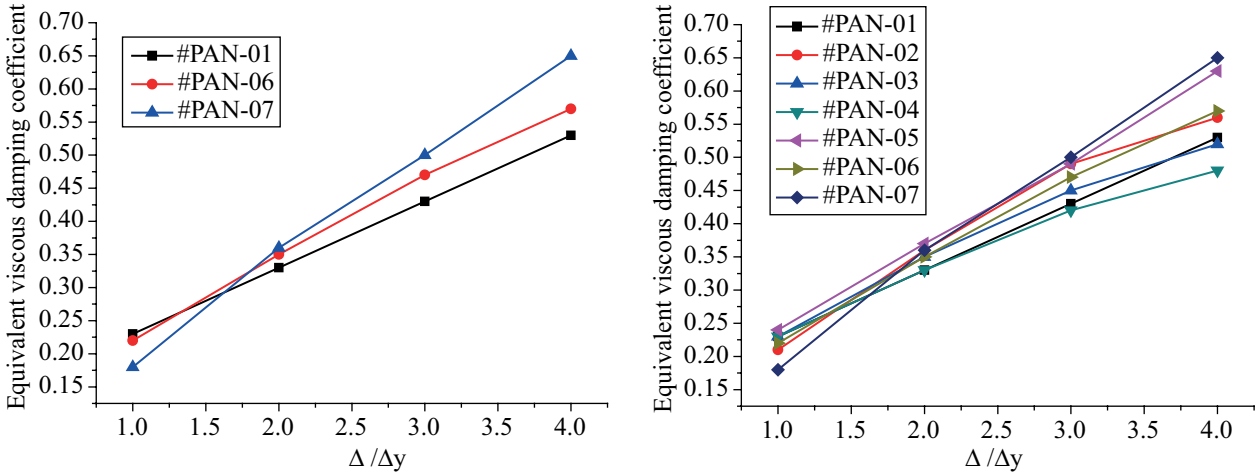

c) Comparison of the equivalent viscous damping coefficients with the different axial pressure ratios

d) Comparison of the equivalent viscous damping coefficients of all the specimens

Figure 5. Comparison of the equivalent viscous damping coefficients.

concrete can effectively improve the energy dissipation capacity of the structure. It can be seen from the comparison chart of the equivalent viscous damping coefficient under the different axial pressure ratios that with an increase in the axial pressure ratio, the equivalent viscous damping coefficient shows an obvious upward trend.

Node stress analysis

Influence of the different axial compression ratios

Under the different axial compression ratios, the stress nephogram of each component is shown in Figure 6.

It can be seen from Figure 6 that a change in the axial compression ratio has little effect on the overall concrete components. From the stress nephogram of the steel beam and end plate, the failure mainly occurs at the connection of the steel beam and the supporting steel pipe, the bolt hole at the connection of the steel beam and the concrete beam, and the upper and lower flanges of the steel beam near the end plate, which belong to bending failures. The main reason is that the stiffness of the connection of the steel beam and supporting steel pipe suddenly decreases. The stress concentration is prone to occur at the bolt hole at the connection of the steel beam and concrete beam. Generally, the composite beams have similar failure characteristics with the change in the axial compression ratio. With an increase

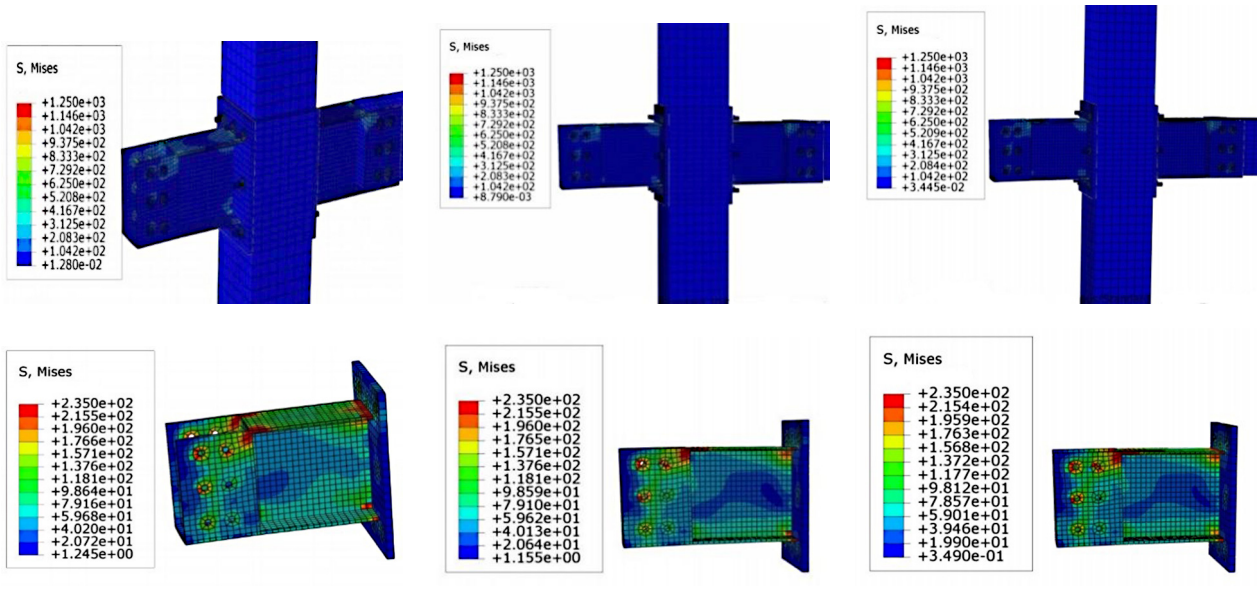

a) Axial compression ratio is 0.3

b) Axial compression ratio is 0.5

c) Axial compression ratio is 0.7

Figure 6. Stress nephogram of each part of the node under different axial compression ratios. *(Continue on next page)*

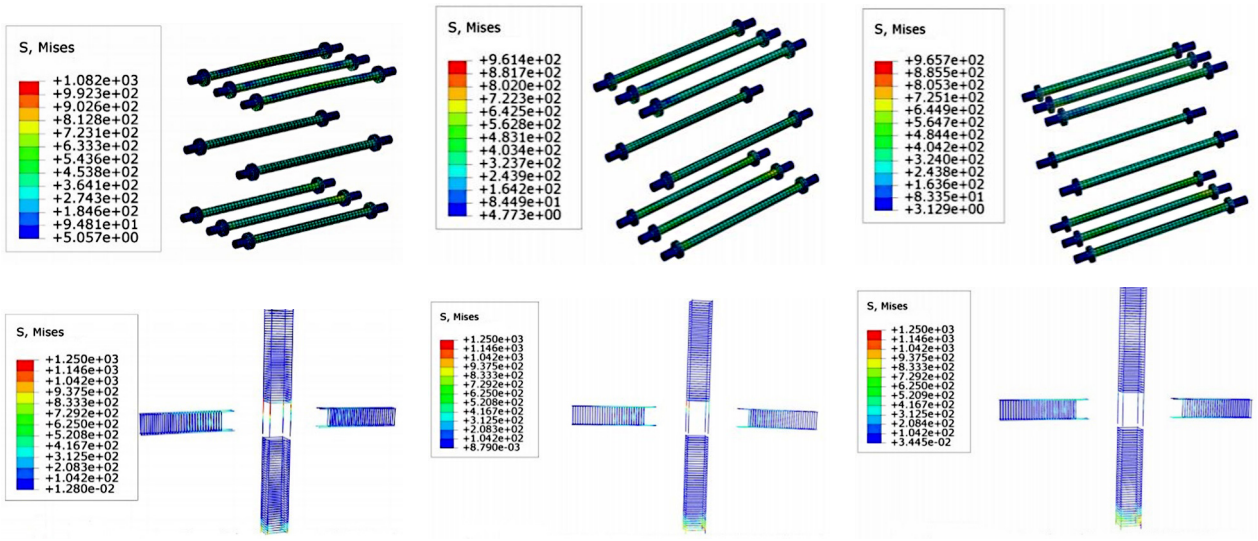

a) Axial compression ratio is 0.3 b) Axial compression ratio is 0.5 c) Axial compression ratio is 0.7

Figure 6. Stress nephogram of each part of the node under different axial compression ratios.

in the axial compression ratio, the bolt stress shows an increasing trend, but not an obvious one. The bolt is in a yield state as a whole.

Effects of the different concrete strengths

Under different concrete strength grades, the stress cloud diagram of each component is shown in Figure 7.

From Figure 7, with a change in the concrete strength grade, the failure form of the steel beam web changes, and the stress on the flange also changes. This indicates that a change in the concrete's strength can cause a change in the structural failure form. In addition, with an increase in the concrete strength grade, the maximum bolt stress showed a downward trend, and the

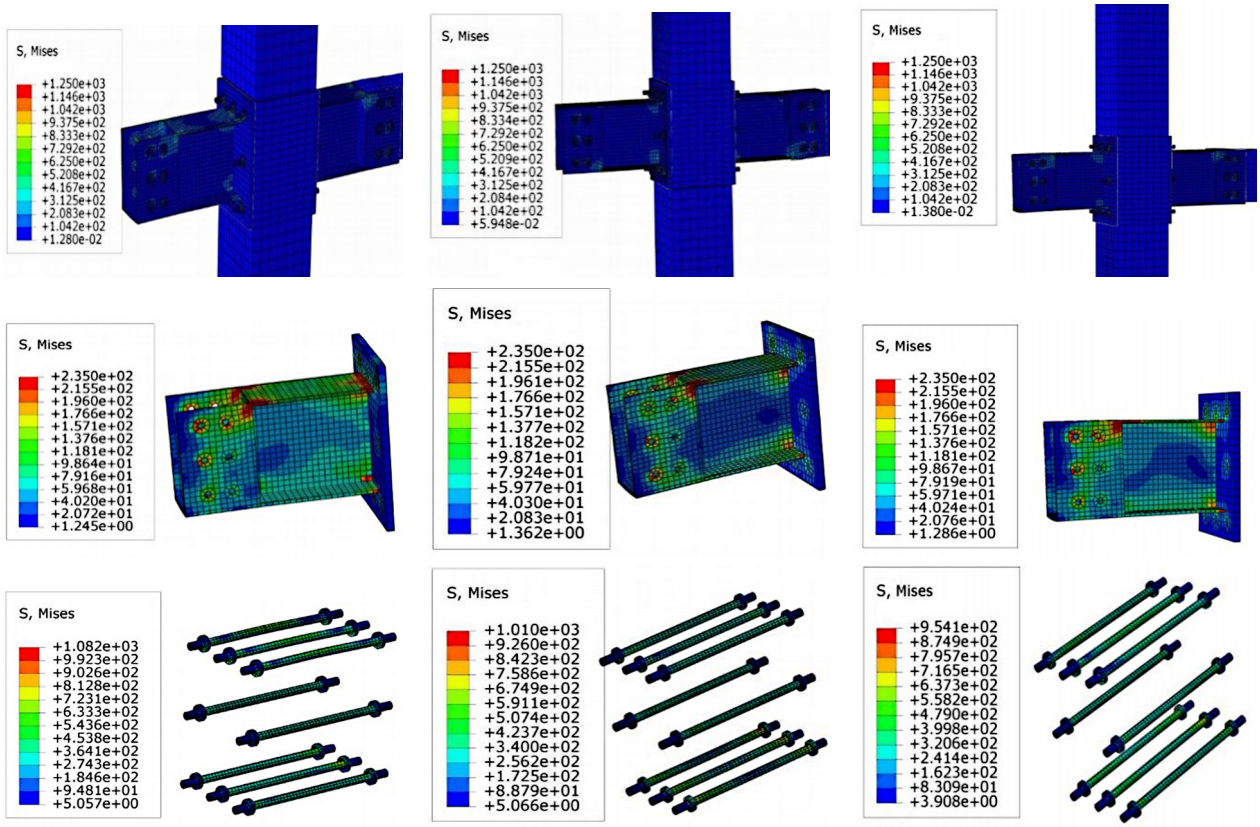

a) Concrete strength grade C30 b) Concrete strength grade C40 c) Concrete strength grade C50

Figure 7. Stress cloud diagram of the different concrete strengths. *(Continue on next page)*

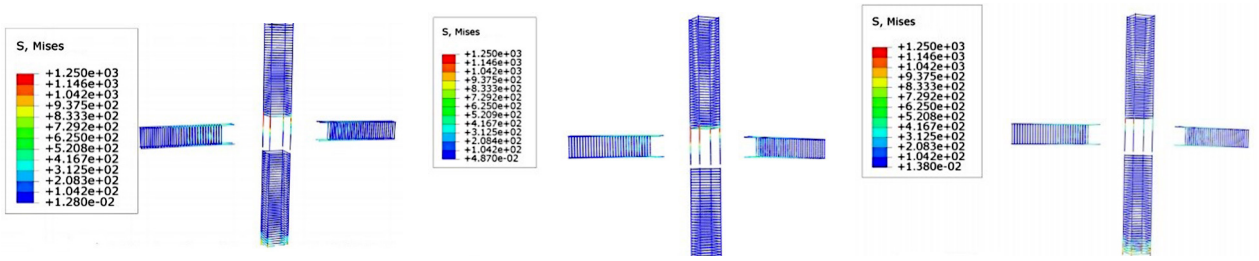

a) Concrete strength grade C30 b) Concrete strength grade C40 c) Concrete strength grade C50

Figure 7. Stress cloud diagram of the different concrete strengths.

change in the concrete strength grade has basically no effect on the steel skeleton.

Influence of the different bolt preloads

Under different bolt preloads, the stress cloud diagram of each component is shown in Figure 8.

It can be seen from Figure 8 that with an increase in the bolt preload, the failure of the steel beam web near the end plate becomes more and more obvious. The failure form of the steel beam has also changed to a certain extent. The higher the preload, the more the failure face extends away from the column end. In addition, with an increase in the bolt preload, the stress

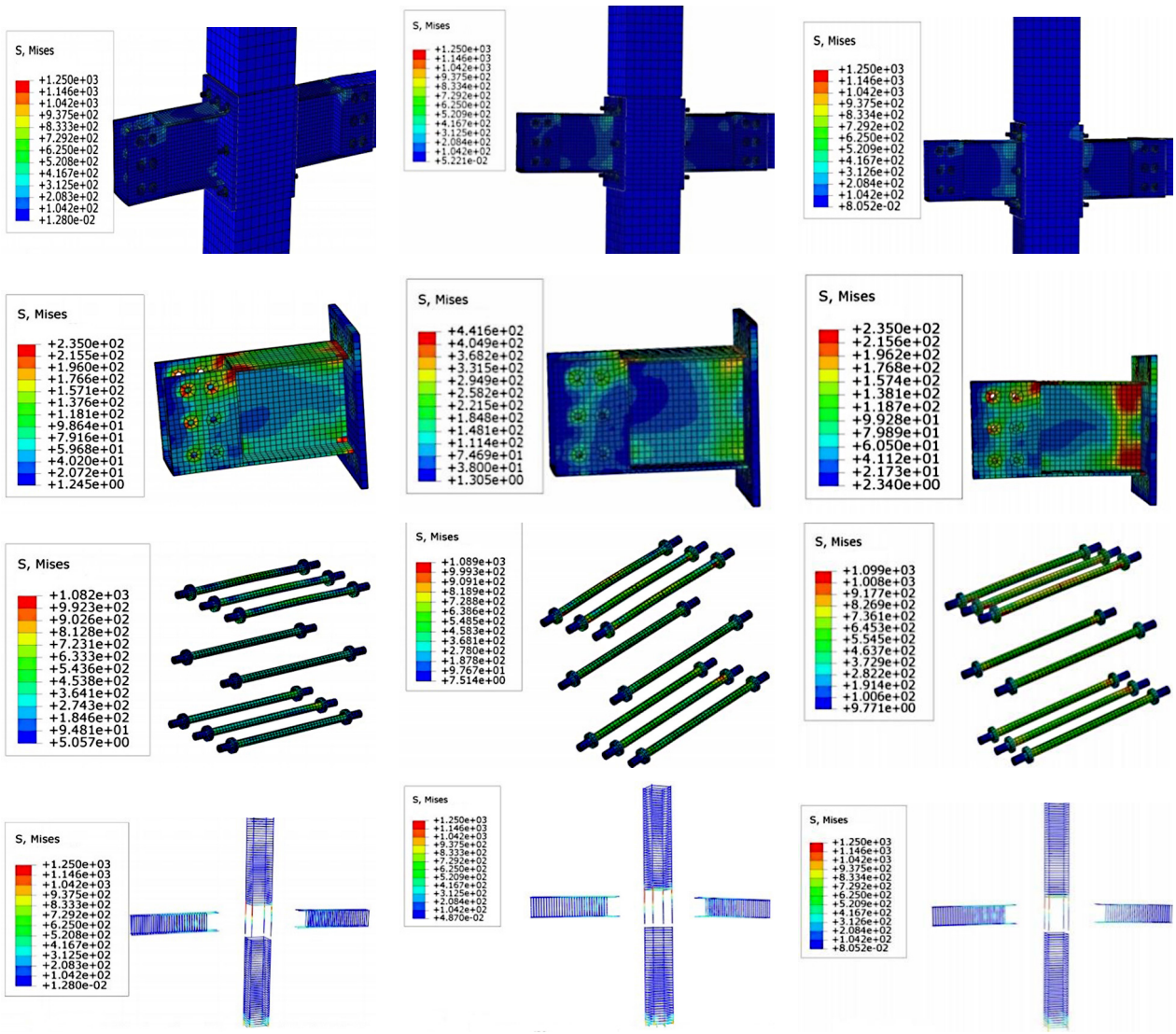

a) Bolt preload of 200 kN b) Bolt preload of 300 kN c) Bolt preload of 400 kN

Figure 8. Stress cloud diagram of the different bolt preloads.

of the high-strength bolts at failure also increases. When the bolt preload reaches 400 kN, the failure at the bolt hole at the connection of the steel beam and concrete beam is relatively obvious.

Analysis of the shear capacity of the nodal domain of the prefabricated CFST composite frame structure

The node domain of the prefabricated CFST composite frame structure proposed in this paper is mainly composed of core concrete, steel pipes and high-strength bolts. The role that they play is due to their respective material properties and they make a great contribution to the bearing capacity of the core area of the node. Due to the steel pipe and bolt preload, the stress state of the concrete in the core area is complex, and its shear bearing capacity is improved. In addition, the steel pipe can provide certain shear resistance. Based on the research results of similar nodes and combined with the characteristics of the node, the factors affecting the shear capacity of the core area of the node can be divided into the contribution of the concrete-filled steel tube, the restraint effect of the bolt preload and the axial pressure on the core concrete, and the contribution of the steel hoop.

Contribution of the core concrete

The relevant experiments and theoretical analysis show that the compressive strength of the oblique bar determines the bearing capacity of the core concrete of the node, and the horizontal component force it bears is the contribution capacity of the concrete to the shear. It can be seen from the mechanism of the oblique bar that when the concrete in the core area cracks, although the core area of the node is not equipped with shear reinforcement, the cracks will not develop excessively due to the effective restraint of the steel plate hoop and bolt preload. However, because the preload of the steel pipe and bolts can be well restrained, the concrete continues to play the role of the oblique bar effectively. According to the force mechanism of the oblique bar [18-19], the contribution of the concrete in the core area of the node to the shear bearing capacity is expressed by the following formula:

$$V_{cu} = 0.8 f_{cc} b_c h_d \cos\varphi \text{ N} \tag{1}$$

$$\cos\varphi = \frac{b_c}{\sqrt{b_c^2 + h_d^2}} \tag{2}$$

where f_{cc} is the compressive strength of restrained concrete, which mainly considers the constraining effect of the steel plate hoop and the combined effect of the bolt preload and the axial force of the column. φ is the angle between the line connecting the bolt centre of the end plate in the compression area on one side and the bolt centre in the tension area corresponding to the back of the column and the horizontal direction b_c mm is the column section width, and h_d mm is the distance of the outermost row of bolts.

Contribution of the steel pipes to the concrete

According to the unified theory of CFST, it can be found that the compressive strength value of CFST is [20]:

$$f_1 = (1.212 + B_S \delta + C_S \delta^2) f_c \text{ Mpa} \tag{3}$$

where the calculation of coefficients B_S and C_S are as follows:
Square and rectangular sections:

$$B_S = 0.131 f_y / 235 + 0.723 \tag{4}$$

$$C_S = -0.07 f_{ck} / 20 + 0.0262 \tag{5}$$

δ can be determined by Formula (6),

$$\delta = \frac{f_y A_s}{A_c} \text{ MPa} \tag{6}$$

where f_y is the yield strength of steel; f_c is the standard compressive strength of concrete; δ is the hoop coefficient; A_s is the area of steel pipe; A_c is the area of the concrete, and α is the steel content.

Contribution of the bolt preload and column axial force to the concrete

According to the Kuperfer-Gerstle yield criterion [21], under the bolt preload and column axial force, the calculation formula of the core concrete strength can be expressed as:

$$f_{cc} = -\frac{1+3.65a}{(1+\alpha)^2} f_c \text{ MPa} \tag{7}$$

$$\alpha = \frac{\sigma_1}{\sigma_2} \tag{8}$$

where σ_1 is the vertical compressive stress of the concrete. According to the axial stiffness distribution principle of a concrete-filled steel tubular column, σ_2 is the lateral compressive stress generated by the bolt preload, and its calculation is:

$$\sigma_1 = N \bullet \frac{E_c A_c}{E_s A_s + E_c A_c} \bullet \frac{1}{A_c} \text{ MPa} \tag{9}$$

$$\sigma_2 = \frac{P}{b_c h} \text{ MPa} \tag{10}$$

where P is the sum of the bolt preload.

From the above analysis, the compressive strength of core concrete can be expressed as:

$$f_{cc} = f_1 + f_2 = \left[\left(1.212 + B\delta + C\delta^2\right) + \frac{1+3.65\alpha}{\left(1+\alpha^2\right)} \right] f_c \text{ MPa} \tag{11}$$

Let $\gamma = (1.212 + B\delta + C\delta^2) + (1 + 3.65\alpha)/(1 + \alpha^2)$, then the shear bearing capacity of the concrete in the core area of the prefabricated CFST composite frame node can be expressed as:

$$V_{cu} = 0.8\gamma f_c b_c h_d \cos\varphi \text{ N} \quad (12)$$

where γ comprehensively reflects the shear resistance of the node core concrete under the constraints of the node steel plate hoop, the bolt preload and axial pressure of the column.

Shear resistance of the steel pipe

The steel pipe in the core area of the node has an excellent constraining effect on the core concrete and can improve its compressive strength. In terms of its shear resistance, it also has a great impact on the shear bearing capacity of the core area of the node [22]. Based on the coordinated deformation of the steel tube and concrete, the shear force of the steel tube is mainly borne by the side steel tube. The ultimate shear stress state of the steel pipe synchronously changes with the shear limit state of the nodal domain. The force diagram of the side steel pipe is shown in Fig. 9, and the steel pipe is in a state of shear compression. Among them, τ is the shear stress of the steel pipe, and σ_{SN} is the axial compressive stress of the steel pipe.

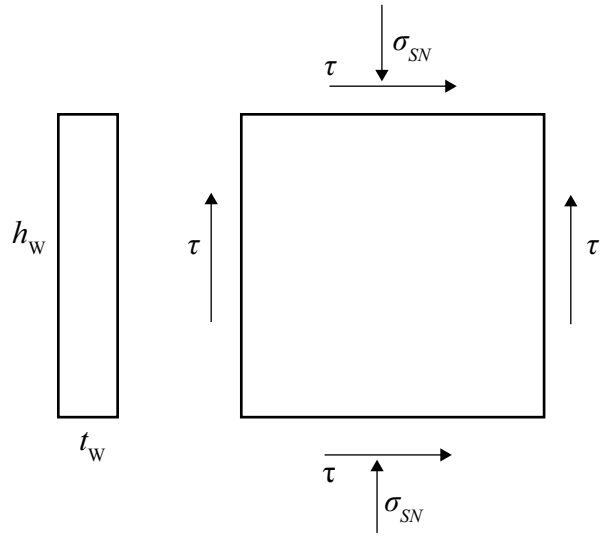

Figure 9. Schematic diagram of the stress state of the steel pipe.

Before yielding, the steel plate hoop is in the elastic stage, and the principal tensile stress is given by

$$\sigma_1 = \frac{\sigma_{SN}}{2} + \sqrt{\left(\frac{\sigma_{SN}}{2}\right)^2 + \tau^2} \quad (13)$$

The principal compressive stress can be expressed as

$$\sigma_1 = \frac{\sigma_{SN}}{2} - \sqrt{\left(\frac{\sigma_{SN}}{2}\right)^2 + \tau^2} \quad (14)$$

When the node reaches the limit state, according to the fourth strength theory of material mechanics, the steel beam web is in a state of shear flow, and the shear yield condition at this time is:

$$\sqrt{\sigma_1^2 + \sigma_2^2 - \sigma_1\sigma_2} \le f_{ya} \quad (15)$$

where: f_{ya} is the uniaxial tensile ultimate strength of the steel pipe.

Combining Formulas (13), (14) and (15), the shear yield stress of the steel pipe can be obtained as:

$$\tau = \sqrt{f_{ya}^2 - \sigma_{SN}^2} / \sqrt{3} \text{ MPa} \quad (16)$$

Then the formula of the shear capacity of the steel pipe can be expressed as:

$$V_s = \tau_s \sum t_w h_w = \frac{\sqrt{f_{ya}^2 - \sigma_{SN}^2}}{\sqrt{3}} \sum t_w h_w \text{ N} \quad (17)$$

$$\sigma_{SN} = N \bullet \frac{E_s A_s}{E_s A_s + E_c A_c} \bullet \frac{1}{A_s} \text{ MPa} \quad (18)$$

where: f_{ya} is the ultimate tensile strength of the steel pipe in one direction; σ_{SN} is the axial compressive stress from the column on the steel pipe; $\sum t_W h_W$ is the area of the steel pipe along the shear direction; t_W is the thickness of steel pipe, and h_W is the length of the surface steel pipe.

Based on the above analysis of the shearing effect of the core concrete and steel pipe, the shear bearing capacity of the core area of the prefabricated CFST composite frame node is as follows:

$$\begin{aligned} V_j &= V_{cu} + V_s \\ &= 0.8\gamma f_c b_c h_d \cos\varphi + \frac{\sqrt{f_{ya}^2 - \sigma_{SN}^2}}{\sqrt{3}} \sum t_w h_w \text{ N} \end{aligned} \quad (19)$$

A total of seven finite element models of this structure have been completed in this paper, and the comparison between the obtained and theoretical values calculated by Formula (19) is shown in Table 3.

From Table 3, the average value of the ratio of the calculated theoretical value to the simulated test value is 1.10. The variance is 0.09, and the coefficient of variation is 8.72%. From the data, the calculated results are basically consistent with the simulation results. Therefore, the formula for the shear capacity of the core area of the node proposed in this paper is reasonable.

CONCLUSION

- The ductility coefficient of this node is basically in the range of 2.02 - 5.75, which is generally higher than 3.0 and has good deformation ability. In addition, this node's equivalent viscous damping coefficient is higher than 0.35, showing optimal energy dissipation capacity and seismic performance.

Table 3. Comparison of the simulated and theoretical values.

Specimens	Strength grade	σ_{SN} Mpa	h_w mm	t_w mm	f_{ya} Mpa	V_e kN	V_c kN	V_c/V_e
#PAN-01	C30	28	710	10	235	7004	6441	0.91
#PAN-02	C30	28	710	10	235	6095	6434	1.05
#PAN-03	C30	26	710	10	235	6153	6434	1.04
#PAN-04	C40	28	710	10	235	5646	6430	1.13
#PAN-05	C50	28	710	10	235	5333	6428	1.21
#PAN-06	C30	41	710	10	235	6095	6405	1.19
#PAN-07	C30	65	710	10	235	6153	6386	1.18
						Average value		1.10
						Standard deviation		0.09
						Coefficient of variation		8.72%

- Using high-strength concrete, the ability of the structure to resist deformation will be weakened, and the energy dissipation capacity of the structure will be improved effectively. High axial compression can improve the stiffness of the structure in the early stage, but it will have an adverse effect in the later stage. In a certain range, increasing the bolt preload can significantly improve the energy dissipation capacity of the structure, and excessive bolt preload has little effect. When the axial pressure ratio increases, the equivalent viscous damping coefficient shows an obvious upward trend.
- From the stress nephograms under different parameters, it can be seen that with an increase in the axial compression ratio, the bolt stress shows an increasing trend, but not an obvious one. With a change in the concrete strength grade, the failure form of the steel beam web changes and the stress on the flange also changes. Therefore, the change in the concrete strength can cause a variation in structural failure form. In addition, the maximum bolt stress shows a decreasing trend with an increase in the concrete strength grades.
- According to the theory of oblique bars, the unified theory of concrete-filled steel tubes and the Kupfer-Gerstle yield criterion, the formula for calculating the shear capacity of the core area of this node is proposed. The theoretical results are compared with the finite element results, and they are in good agreement.

Acknowledgement

This research was supported by the Department of Science and Technology of Henan Province through Grant No. 212102310971. The financial support is highly appreciated.

REFERENCES

1. Ajith M. S., Beena K. P., Sheela S. (2021): Hysteresis Performance of Through Bolted Connections in Steel Beam to Circular CFST Column. *KSCE Journal of Civil Engineering, 25*(7), 2487-2500. Doi: 10.1007/s12205-021-0488-9
2. Kukla D., Kozlowski A. (2021): Parametric study of steel flush and extended end-plate joints under column loss scenario. *Engineering Structures, 237*, 112204. Doi: 10.1016/j.engstruct.2021.112204
3. Díaz C., Victoria M., Querin O. M., Martí P. (2018): FE model of three-dimensional steel beam-to-column bolted extended end-plate joint. *International Journal of Steel Structures, 18*(3), 843–867. Doi: 10.1007/s13296-018-0033-y
4. Van Long H., Jaspart J. P., Demonceau J. F. (2016): Use of long bolts for beam-to-concrete-flled rectangular hollow section column joints in seismic-resistant frames. *Steel construction, 9*(4), 305-314. Doi: 10.1002/stco.201610037
5. Al Fakih K., Chin S. C., Doh S. I. (2018): Behavior of extended end-plate steel beam to column connections. *The Open Civil Engineering Journal, 12*(4), 250-262. Doi: 10.2174/1874149501812010250
6. Ismail R. E. S., Fahmy A. S., Khalifa A. M., Mohamed Y. M. (2016): Numerical study on ultimate behaviour of bolted endplate steel connections. *Latin American Journal of Solids and Structures, 13*(1), 1-22. Doi: 10.1590/1679-78251579
7. Tartaglia R., D'Aniello M., Rassati G. A. (2019): Proposal of AISC-compliant seismic design criteria for ductile partially-restrained end-plate bolted joints. *Journal of Constructional Steel Research,159*, 364-383. Doi: 10.1016/j.jcsr.2019.05.006
8. Tartaglia R., D'Aniello M., Rassati G. A., Swanson J. A., Landolfo R. (2018): Full strength extended stiffened end-plate joints: AISC vs recent European design criteria. *Engineering Structures, 159*, 155-171. Doi: 10.1016/j.engstruct.2017.12.053
9. Wang X. T., Hao J. P., Zhou G. G.(2009): Hysteretic Behavior of High Strength Bolts-End-plate Connections for Concrete Filled Square Steel Tubular Columns. *Progress in Steel Building Structures, 11*(1), 33-37.
10. Wang X. T., Zhou C., Ma Y. S. F., Yang H. D., Wang L.Q. (2014): Study on restoring force model of concrete filled square steel tube planar frames. *Earthquake Engineering and Engineering Dynamics, 34*(5), 94-99. Doi: 10.13197/j.eeev.2014.05.94.wangxt.013
11. Li S. C., Yan J., Wang H. L. (2009): Pseudo-static test research on concrete column-honeycombed steel beam composite joints. *Journal of Building Structures, 30*(2), 30-38. Doi: 10.14006/j.jzjgxb.2009.02.016
12. Ding C.T., Pan X.B., Bai Y., Shi G. (2019): Prefabricated connection for steel beam and concrete-filled steel tube column. *Journal of Constructional Steel Research, 162,* 105751. Doi: 10.1016/j.jcsr.2019.105751

13. Wang Q., Lu J., Hou K., Yin Z. P. (2018): Study of Material Constitutive Model for Shear Wall Hysteretic Behavior Analysis. *Journal of Shenyang Jianzhu University (Natural Science), 34*(3), 402-409. Doi: 10.11717/j.issn:2095 -1922. 2018.03.03
14. Zhang W. Y., Chen Y. Y. (2017): Effect of the Hardening Parameters in Steel Constitutive Models on the Hysteretic Behavior of Structural Members. *Progress in Steel Building Structures, 19*(1), 10-16. Doi: 10.13969/j.cnki.cn31-1893. 2017.01.002
15. GB50010-2010.(2010): Code for Design of Concrete Structures. China Architecture and Building Press, Beijing, China (in Chinese).
16. Kalmykova S. (2021): Simulation of T-Joints between RHS Steel Members with Offset in Abaqus. *Acta Polytechnica CTU Proceedings, 30*, 36-40. Doi: 10.14311/APP.2021. 30.0036
17. Chen H. B., Zhou Y. J., Nan G. (2017): Seismic Performance Research for L-shaped Column Joint with Concrete Filled Steel Pipe Based on ABAQUS Software. *Earthquake Resistant Engineering and Retrofitting, 39*(2), 24-29. Doi: 10. 16226/j.issn.1002-8412.2017.02.004
18. Liu M., Wu T., Xing G. H., Zhang B. L., Liu B. Q. (2011): Parameter study on shear behavior of RC interior joints with different depth beams using equivalent strut mechanism. *China Civil Engineering Journal, 44*(S1), 1-7. Doi: 10.15951/j.tmgcxb.2011.s1.029
19. Zhang X. Z., LiX. Q., Zhang S. H., Zhang T. H., Yan X. Y., Yu Z. S.(2022):Mechanical Behavior Analysis of Panel Zone in Concrete-Filled Precast Concrete Tube Column-to-Steel Beam Connections. *Journal of Tianjin University (Science and Technology), 55*(4), 428-440. Doi: 10.11784/ tdxbz202103049
20. Wu H. P., Cao W. L., Dong H. Y. (2019): Axial Compressive Strength Calculation Based on the Unified Theory for Special-Shaped CFT Columns with Multiple Cavities. *Engineering Mechanics, 36*(8),114-121. Doi: 10.6052/j.issn. 1000-4750.2018.07.0397
21. Kupfer H. B., Gerstle K. H. (1973): Behavior of concrete under biaxial stress. *Journal of the Engineering Mechanics Division, 99*(4), 853-866. Doi: 10.1061/JMCEA3.0001789
22. Men J. J., Li H. J., Wang X. D., Guan R.R., Guo Z. F. (2014): Research on shear bearing capacity of reinforced concrete column-steel beam composite joint. *Building Structure, 44*(6), 74-78. Doi: 10.19701/j.jzjg.2014.06.018